Determination of Isotherms for Binding of Surfactants to Vesicles Using a Surfactant-Selective Electrode

M. Kadi,*,† P. Hansson,‡ and M. Almgren†

Department of Physical Chemistry, Uppsala Biomedical Centre, P.O. Box 579, SE-751 23 Uppsala, Sweden, and Department of Pharmacy, Uppsala Biomedical Centre, P.O. Box 580, SE-751 23 Uppsala, Sweden

Received: January 12, 2004; In Final Form: March 19, 2004

Mixtures of the nonionic lipid glycerol monooleate with four cationic surfactants have been investigated. The surfactants were cetyltrimethylammonium chloride, tetradecyltrimethylammonium chloride, and dodecyltrimethylammonium chloride, and one with a partially fluorinated chain, *N*-(1,1,2,2-tetrahydroperfluorodecanyl)-pyridinium chloride. With a low addition of the cationic surfactant, GMO easily forms vesicles. Using a surfactant selective electrode, binding isotherms of the surfactants to a suspension of preformed vesicles were determined. The mole fractions of surfactant at which the micelle−vesicle coexistence region and the micelle region were reached, as obtained from the binding isotherms, were compared to the location of the corresponding phase borders in the phase diagrams of the respective mixtures. The different stages of the solubilization process were directly followed using cryo-TEM. Instead of a micelle−vesicle coexistence region, perforated vesicles were observed during the solubilization with C_{16}TAC. The binding isotherm was nevertheless similar to those of the other surfactants. On the basis of this result, the formation of pores in the bilayer is regarded as a cooperative process, similar to micelle formation. The edges of the pores are richer in surfactant than the intact part of the bilayer. Increasing the surfactant concentration does not change the composition but results in an increased number of pores, similar to a micelle−vesicle phase separation.

Introduction

The surfactant induced transition from vesicles to mixed micelles has been extensively studied for mixtures of nonionic detergents and phospholipids.[1−7] Ionic surfactants, with exception for the biologically relevant bile salts, have attracted less attention.[8−14] The so-called three-stage model has often been used successfully to describe surfactant solubilization of vesicles.[5,7,15,16] Initially, the added surfactant is distributed between the water phase and the vesicles. In the second stage, vesicles coexist with mixed micelles at a constant composition of the aggregates. The vesicles are progressively transformed into mixed micelles and finally, in stage three, only mixed micelles are found in the solution.

A system that deviates from this behavior is GMO/C_{16}TAB in 100 mM NaCl[17] and a few other lipid/surfactant mixtures in which perforated vesicles have been found as intermediate structures during the solubilization.[10,11] Threadlike micelles are formed in those systems, sometimes via sheetlike aggregates, without any visible micelle/vesicle coexistence region. The perforated vesicles originate from a lamellar phase with randomly distributed water-filled pore or channel defects. These defective lamellar phases have been observed in a number of systems, both nonionic and ionic amphiphile systems.[17−27] Their relationship to so-called intermediate phases has been pointed out since both types of phases exist because of the strive for a mean curvature between that of a normal lamellar phase and a hexagonal phase.[18]

Our main interest in this study was to investigate the thermodynamics of surfactant solubilization of vesicles when perforated vesicles are formed as intermediate structures and to compare this to the results for surfactants that follow the more normal route with coexistence of micelles and vesicles. We also studied the binding of a partially fluorinated cationic surfactant to vesicles, to investigate possible effects of the tendency to demixing between fluorocarbon and hydrocarbon chains. Others have studied the thermodynamics of vesicle solubilization using titration calorimetry, which has been shown to be a convenient method for following the different stages of the solubilization process.[28] Surfactant partition coefficients between bilayer and water have also been determined by equilibrium dialysis[14], but this method suffers from the disadvantage of requiring separation of the aggregates from the aqueous medium. Here, we used a surfactant selective electrode to measure the surfactant activity after addition of surfactant to a suspension of preformed vesicles. The data were used to calculate binding isotherms of different cationic surfactants to glycerolmonooleate (GMO)/surfactant vesicles. The following surfactants were studied: C_{16}TAC (cetyltrimethylammonium chloride), C_{14}TAC (tetradecyltrimethylammonium chloride), C_{12}-TAC (dodecyltrimethylammonium chloride), and the partly fluorinated surfactant HFDePC (*N*-(1,1,2,2,-tetrahydroperfluorodecanyl)pyridinium chloride). The different stages of vesicle solubilization were followed by direct observation of the structures using cryo-TEM.

As a complement, we also determined partial phase diagrams (the solvent-rich corner) of GMO/C_{12}TAC and GMO/C_{14}TAC in 100 mM NaCl (the system GMO/ C_{16}TAB in 100 mM NaCl was investigated earlier[17]) to discuss the aggregate structures observed at high dilution and the binding isotherms in relation to the equilibrated phase behavior.

The aggregate structures observed by cryo-TEM during solubilization are different for the three hydrocarbon surfactants,

* Corresponding author. E-mail: mari_kadi@hotmail.com.
† Department of Physical Chemistry.
‡ Department of Pharmacy.

10.1021/jp049848q CCC: $27.50
Published on Web 04/28/2004

but the binding isotherms appear very similar. We try to explain the results by assuming that a demixing of lipids and surfactants occurs within the perforated membrane as proposed earlier.[29] The results for the partially fluorinated surfactant show that it is incorporated into the bilayer to a considerable extent before micelles form, containing only a few percent of GMO. The solubilization route followed by this surfactant is consistent with the three-stage model.

Materials and Methods

Chemicals. C_{16}TAC was prepared by ion exchange from the bromide salt (Serva, analytical grade). C_{12}TAC and C_{14}TAC, analytical grade, were purchased from Fluka and used as received. The cationic fluorinated surfactant HFDePC was a gift from Prof. Asakawa (Kanazawa University, Japan). The synthesis has been described earlier.[30] The fatty acid content of the glycerolmonooleate obtained from Danisco Ingredients, Brabrand, Denmark was as follows: 92% C18:1, 6% C18:2, and 2% saturated acids.

Sample Preparation. Small unilamellar vesicles were prepared by ultrasonic irradiation of samples containing about 10 mg of glycerol monooleate and small amounts of the cationic surfactant under study in 8 mL of 100 mM NaCl solution. GMO forms a reversed bicontinuous cubic phase in water or 100 mM NaCl. Adding a few percent of the cationic surfactant balances the spontaneous curvature toward zero, which allows vesicles to form. A Soniprep 150 from MSE Scientific Instruments, Crawley, UK was used for the irradiation. The samples were then diluted by addition of 100 mM NaCl. Small amounts of a concentrated stock solution of the surfactant were added to obtain the desired concentration. All solutions were filtered through a 0.2 μm Sartorius Minisart filter before the addition of surfactant. The solutions were left to equilibrate for 24 h prior to the investigations. The samples for the phase diagram investigations were prepared by weighing. They were periodically mixed for one week and then left to equilibrate for at least four weeks at 25 °C.

Cryo-TEM. The technique has been described in detail elsewhere.[31,32] A thin sample film spanning the holes in the polymer film covering the copper grid was prepared by adding a small drop of the solution onto the grid and removing excess liquid by blotting using a filter paper. This was done within a controlled environment chamber at 25 °C and with a relative humidity of 98−99% to avoid evaporation of the liquid. By plunging the grid into liquid ethane held just above its freezing point, rapid vitrification of the film was achieved. The sample was then transferred to a Zeiss 902A microscope operating at an accelerating voltage of 80 kV. The temperature was kept below −165 °C during the entire procedure to prevent sample perturbation and formation of ice crystals.

SAXS. A Kratky compact small-angle system with linear collimation was used for the X-ray investigations. The Seifert ID-3000 X-ray generator was operating at 50 kV and 40 mA providing CuKα radiation with a wavelength of 1.54 Å. The samples were contained in a flat cell with mica windows and kept at 25 °C. The OED 50M detector contained 1024 channels and was placed on a distance of 277 mm from the sample.

Surfactant Selective Electrode. The free surfactant concentrations in the vesicle solutions were determined potentiometrically using a surfactant selective membrane electrode. The membrane was prepared following the procedure described by Hayakawa and Kwak[33] except that the carrier complex was left out. The cell used for the measurements was set up as follows:

calomel electrode|agar, 0.5 M NH_4Cl|
test solution|PVC membrane|reference solution|
agar, 0.5 M NH_4Cl|calomel electrode

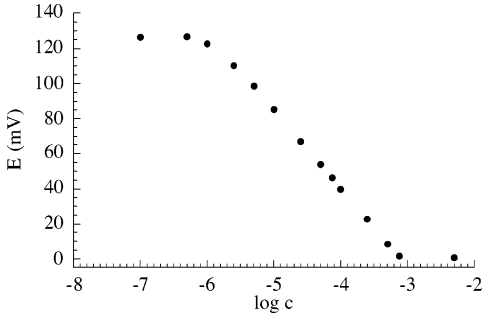

Figure 1. Plot of the emf response of the surfactant selective electrode as a function of C_{14}TAC concentration (the calibration curve). All solutions contained 100 mM NaCl.

The reference solutions were prepared well above the cmc of the surfactant under study in 100 mM NaCl. The potential difference between the reference solution and the test solution placed on different sides of the membrane was measured using a voltmeter with an internal resistance of 10 MΩ, which is substantially larger than the internal resistance of the measuring cell.[34] This potential difference is related to the surfactant monomer concentration in the test solution, and by the use of calibration curves the free surfactant concentration in the vesicle solutions could be determined. These results were then used to construct binding isotherms of the surfactants to the vesicles.

The calibration curves gave slopes of the emf responses that usually were somewhat smaller than the theoretically expected 59 mV. The curve for C_{14}TAC in Figure 1 had a slope in the linear portion of 45 mV, as compared to 55 mV for the calibration curve of C_{12}TAC in ref 34. For HFDePC, the slope was even smaller than for the three hydrocarbon surfactants. The reason is not clear. However, since a reproducible calibration curve was obtained, it did not seem to affect the results. The calibration curves were also used to determine the critical micelle concentrations, which for C_{12}TAC and C_{16}TAC were approximately the same as determined by other methods. For C_{12}TAC in 100 mM NaCl, the cmc was determined as 7.2 mM, the same as determined earlier[35] and for C_{16}TAC 0.068 mM, which agrees well with the value for C_{16}TAC in 100 mM KCl reported earlier.[36] The cmc of C_{14}TAC and HFDePC in 100 mM NaCl were obtained as 0.8 and 0.2 mM, respectively.

DLS. The light source for the dynamic light scattering experiments was an Ar ion laser emitting vertically polarized light at 488 nm. This setup has been described earlier.[37]

Results

Aggregate Structures as Observed by Cryo-TEM. *C_{14}TAC and C_{12}TAC with GMO in 100 mM NaCl.* Aggregates observed with the short-chain surfactants are shown in Figure 2. At low surfactant/lipid ratios, only vesicles were observed (Figure 2a), at higher ratios both globular micelles and vesicles (Figure 2b,c), and finally only micelles (not shown). The normal route predicted by the three-stage model described previously is thus followed. Contrary to the observations in the case of solubilization of EPC−liposomes with the same surfactants,[29] no cylindrical micelles were observed. A similar difference between lecithin and GMO was noted in solubilization with bile salts: only globular micelles with GMO[38] and threadlike micelles with

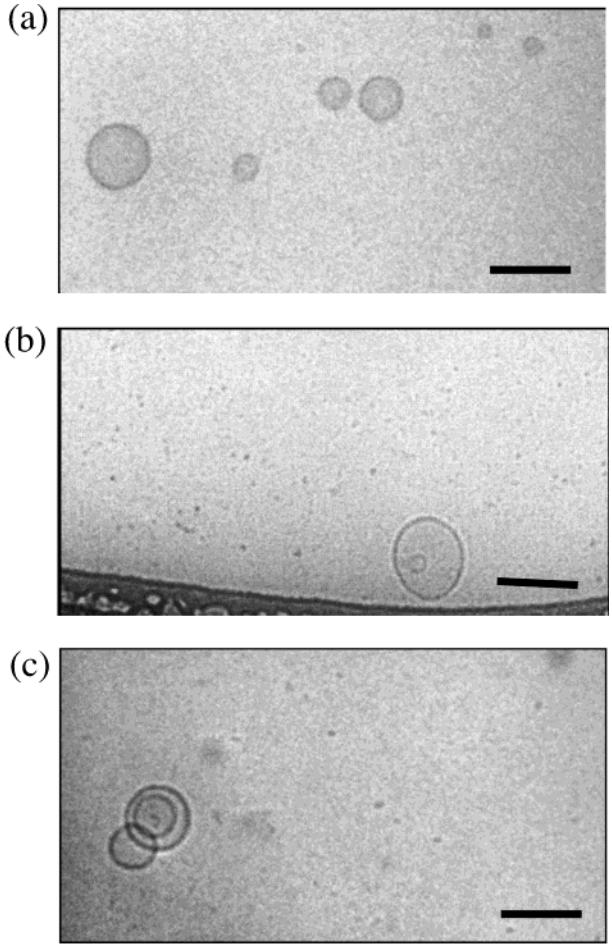

Figure 2. Cryo-TEM micrographs from samples with molar ratio of C_{12}TAC to GMO of 4 (a), 6.4 (b), and at a molar ratio of C_{14}TAC to GMO of 2 (c). The lipid concentration was 1.0 mM, and the concentration of NaCl was 100 mM. Bar equals 100 nm.

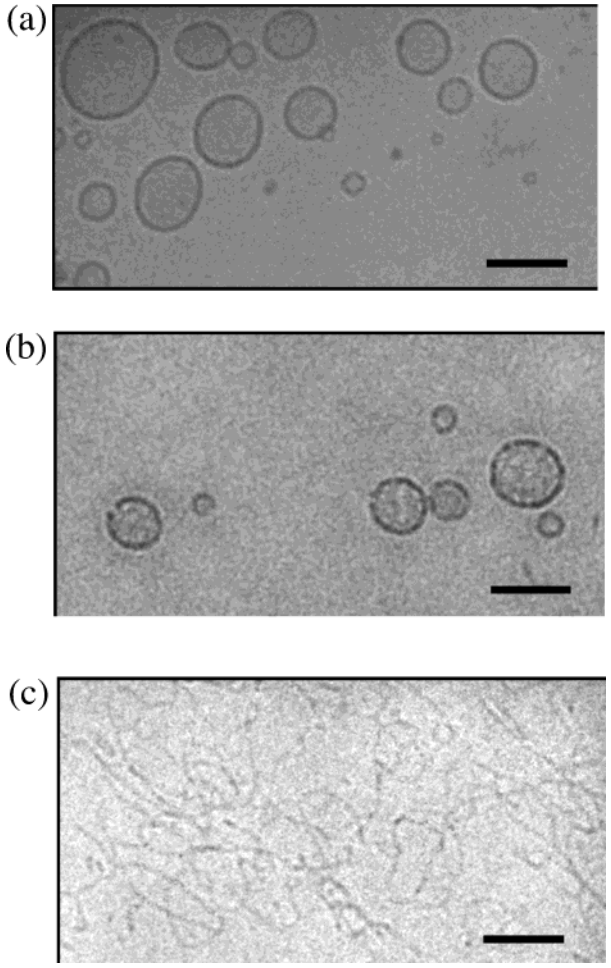

Figure 3. Cryo-TEM micrographs from samples with molar ratio of C_{16}TAC to GMO of 1 (a), 1.7 (b), and 2.3 (c). Bar equals 100 nm. Note the perforated membranes of the vesicles in panel b.

EPC.[39,40] This absence of micellar growth in the GMO-based system is reflected also in the phase diagrams. In the lecithin/bile salt system, a large region in the diagram is occupied by a hexagonal phase,[41] which is not found in the phase diagram of GMO/sodium cholate.[38]

GMO/C_{16}TAC/100 mM NaCl. When the surfactant chain length was further increased, the solubilization characteristics changed dramatically as described earlier.[17] No coexistence of vesicles and micelles could be observed. Instead, the aggregate structure changed continuously from intact vesicles through intermediate structures such as perforated vesicles, threadlike micelles, shorter cylindrical micelles, and finally resulting in small globular micelles. Some intermediate aggregate structures are shown in Figure 3. At low surfactant/lipid ratios, only intact vesicles were found (Figure 3a). The perforated vesicles, composed of holey bilayers, could be observed at molar ratios of approximately 1.7 (Figure 3b). Perforated vesicles were first observed by Hoffmann[19] using freeze-fracture microscopy but have since then been observed in a few systems by cryo-TEM.[10,11,17,18] By the formation of these bilayers with curvature inhomogenities, the mean curvature approaches that of the hexagonal (or micellar) phase, and the molecular packing constraints of the surfactant are better satisfied than in an intact bilayer. This requires the radius of the pore to be sufficiently large for the mean curvature experienced by the molecules at the rim of the pore to be positive.[42] A further increase in surfactant concentration to a surfactant-to-lipid ratio of 2.3 resulted in a transformation of perforated vesicles into threadlike micelles (Figure 3c). The more surfactant added, the shorter the mixed micelles became. The transition from perforated vesicles to threadlike micelles probably occurs through a state with small sheetlike aggregates of interconnected threads as observed earlier.[18,43] It is possible that these aggregates are related to structures in the isotropic flow birefringent fluid phase denoted L_1* in the phase diagram GMO/CTAB/100 mM NaCl.[17]

GMO/HFDePC/100 mM NaCl. The micrograph in Figure 4a showing spherical micelles together with vesicles refers to a sample with a surfactant/lipid ratio of 3. No attempts were made to exactly determine the limit of the coexistence region, but from dynamic light scattering, it was established that micelles and vesicles coexist at least up to a molar ratio of surfactant to lipid of 40. At this surfactant-to-lipid ratio, a broad population of vesicles, possibly bimodal with peak hydrodynamic radii of 11 and 54 nm, was found together with micelles with a hydrodynamic radius of 3 nm. At a molar ratio of 50, threadlike micelles were found, and vesicles could no longer be observed using cryo-TEM (Figure 4b). The micellar growth into cylindrical micelles in this case is a consequence of the presence of HFDePC in the mixed micelles since at this concentration and ionic strength also pure HFDePC forms elongated micelles.[44]

Phase Behavior of GMO/C_xTAC/100 mM NaCl. The solvent corners of the ternary phase diagrams GMO/C_{12}TAC/100 mM NaCl and GMO/C_{14}TAC/100 mM NaCl are shown in Figure 5a,b. The samples were investigated by visual inspection in normal light and between crossed polarizers to detect optical anisotropic phases (lamellar and hexagonal).

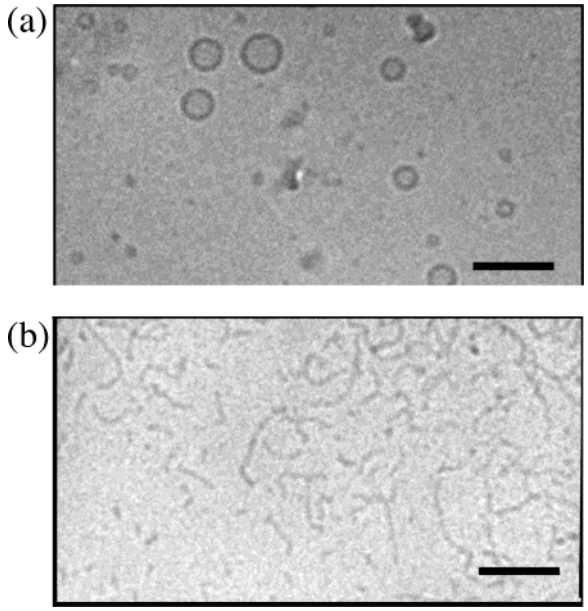

Figure 4. Cryo-TEM micrographs from samples with molar ratio of HFDePC to GMO of 4 (a) and 50 (b). Bar equals 100 nm.

The micellar cubic phase denoted I_I (space group *Pm*3*n*) was identified in both systems by the characteristic SAXS profile with the relative position of the dominant peaks $\sqrt{4}$:$\sqrt{5}$:$\sqrt{6}$. This structure was earlier observed in egg lecithin/ C_{12}TAC/ 100 mM NaCl[29] as well as in the binary phase diagram of C_{12}-TAC in water.[45,46] Close to this region, the micelles are small as judged from the viscosity of the samples. The hexagonal phase was identified by a reflection pattern showing three peaks with the relative position 1:$\sqrt{3}$:$\sqrt{4}$. Between the hexagonal and the micellar phase, two-phase regions were observed.

The repeat distances as obtained from SAXS measurements changed upon dilution of the lamellar phases at fixed compositions of C_{12}TAC and C_{14}TAC in GMO (Figure 6). The straight lines are calculated for ideally swelling bilayers. The bilayer thickness was calculated from the most concentrated sample with the density of the amphiphile mixture as well as the density of the brine approximated to 1 g/mL:

$$d = \frac{2v_s}{a_s\Phi} = \frac{\delta}{\Phi} \qquad (1)$$

where v_s is the average molecular volume of the amphiphiles, and a_s is the average molecular area of the amphiphiles in the bilayer. δ is the effective bilayer thickness, and Φ is the volume fraction of amphiphiles. Close to ideal swelling behavior was found for GMO/C_{12}TAC. The deviations were somewhat larger in C_{14}TAC/GMO where the observed distance is approximately 8% smaller than calculated for ideal swelling at high dilution. A much stronger negative deviation, at least 30%, was earlier found for both EPC/C_{16}TAC[18] and GMO/C_{16}TAC[17] and was explained by an increase of the bilayer area upon dilution due to the formation of water-filled pores in the lamellar structure. The swelling behavior suggests that the lamellar phases found with the shorter-chain surfactants have intact bilayers. Instead of a bilayer with curvature defects as with C_{16}TAC, there is now a large two-phase area. The two-phase area between the micellar (or hexagonal) phase and the lamellar phase is somewhat wider with C_{14}TAC than with C_{12}TAC as surfactant. This is mainly due to the fact that the micelles can accommodate more of the lipid in the case of the short-chain surfactant, whereas the destabilization of the lamellar phase occurs at almost the same molar surfactant-to-lipid ratio in both cases; see Table 1. The equilibrium compositions of the two coexisting phases have not been determined. At relatively low water content, the lamellar phase coexists with a hexagonal phase and at higher dilution with a micellar phase.

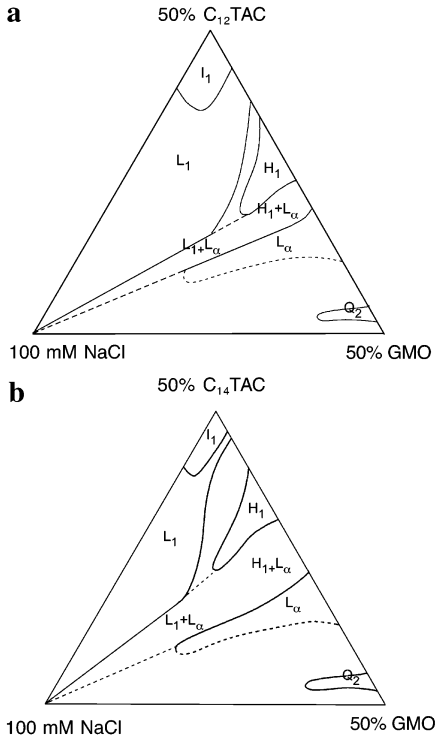

Figure 5. Solvent corner of the phase diagrams (a) GMO/C_{12}TAC/ 100 mM NaCl and (b) GMO/C_{14}TAC/100 mM NaCl. L_α denotes the lamellar phase, and L_1, H_1, and I_1 denote the micellar, hexagonal, and micellar cubic phases, while Q_{II} denotes the reverse bicontinuous cubic phase. Note that all multiphase regions are not outlined in the diagrams.

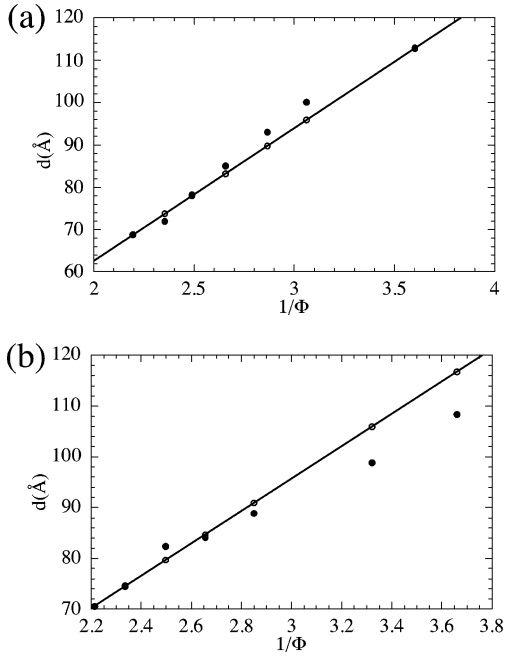

Figure 6. Observed lamellar repeat distance (filled circles) as a function of the inverse volume fraction of amphiphiles for a series with (a) molar ratio C_{12}TAC/ GMO = 0.70 and (b) C_{14}TAC/GMO = 0.67. The empty circles connected by the straight line correspond to the calculated values for an ideally swelling bilayer with the apparent bilayer thickness taken to be equal to the bilayer thickness of the most concentrated sample.

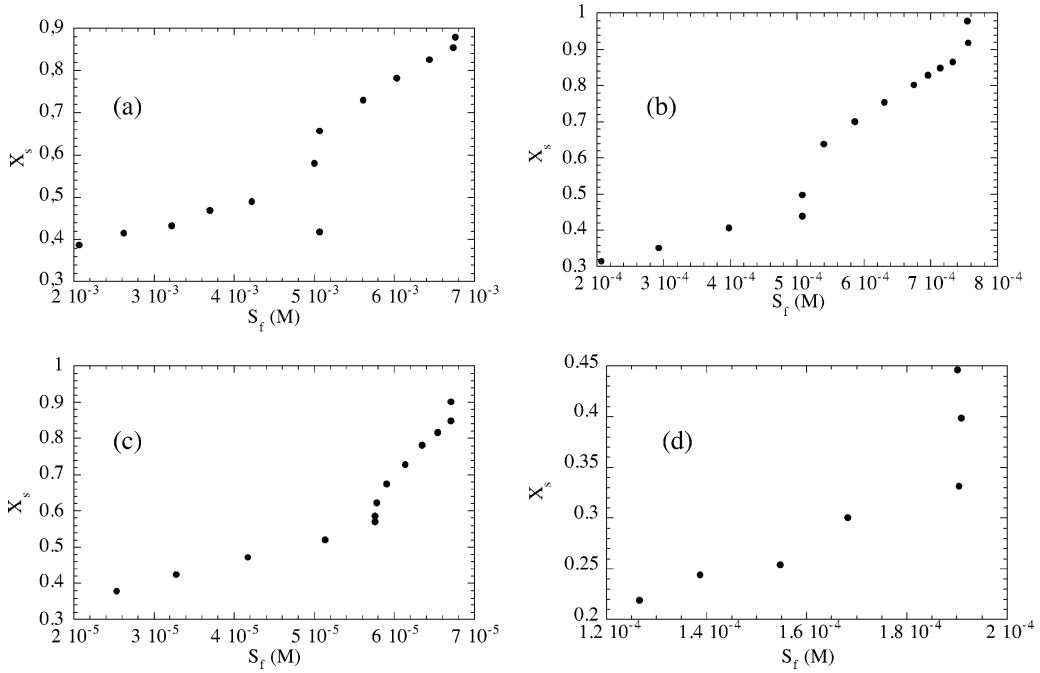

Figure 7. Binding isotherms of (a) C_{12}TAC, (b) C_{14}TAC, (c) C_{16}TAC, and (d) HFDePC to preformed GMO vesicles. The mole fraction of surfactant in the structures is plotted as a function of the free surfactant concentration in the aqueous phase. The GMO concentration was 1.0 mM, and the NaCl concentration was 100 mM.

TABLE 1: Values of cmc, the Bilayer Partitioning Coefficients K_b, X_s^{sat}, and X_s^{sol} Determined from the Phase Diagrams[a]

surfactant	cmc[b]/(10^{-3} M)	K_b/M^{-1}	X_s^{sat}	X_s^{sol}
C_{12}TAC	7.2 (8.4)	50	0.46	0.57 (0.66)
C_{14}TAC	0.80 (0.85)	420	0.47 (0.44)	0.67 (0.64)
C_{16}TAC	0.068 (0.045)	5400	0.57 (0.57)	0.71 (0.70)
HFDePC	0.20	1800	(0.33)	(≈0.97)

[a] Values obtained from the binding isotherms are within brackets. X_s^{sat} for C_{16}TAC refers to the surfactant to lipid ratio at which the defective lamellar phase is entered. [b] From calibration curve in 100 mM NaCl.

The SAXS scattering profile from the optically clear reversed bicontinuous cubic phase (Q_{II}) found at low surfactant/lipid molar ratio is compatible with space group *Ia*3*d*. This structure was also observed in the study of GMO/C_{16}TAB/100 mM NaCl, although the *Pn*3*m* structure seemed to be dominating in this case.[17] This bicontinuous cubic phase can swell to approximately 58 wt% 100 mM NaCl and 60 wt% 100 mM NaCl, respectively, when it contains a few percent of C_{12}TAC.

Binding Isotherms. Binding isotherms of C_{12}TAC, C_{14}TAC, C_{16}TAC, and HFDePC to GMO vesicles in 100 mM NaCl are presented in Figure 7. The amount of bound surfactant was calculated by subtraction of the free surfactant concentration, as measured by the surfactant selective electrode, from the known total surfactant concentration. The lipid concentration was in all experiments 1.0 mM.

In the first region of the binding isotherm of C_{12}TAC (shown in Figure 7a) and C_{14}TAC (shown in Figure 7b), the surfactant molecules distribute between bilayers and water so that the amounts of both bound and free surfactant increase nearly linearly with increasing total surfactant concentration. From the slope of the curve in this regime, a membrane partition coefficient can be calculated as shown below.

When the micelle−vesicle coexistence region (region 2) is entered, the slope of the curve changes abruptly and becomes almost vertical, consistent with the three-stage model, in which it is assumed that the compositions of the bilayers and the micelles, given by X_s^{sat} and X_s^{sol} are fixed during the solubilization. The chemical potential of the surfactant, and hence the free surfactant concentration, should remain constant from the point where micelles first appear until all the bilayers have disappeared. (In many systems, however, the free surfactant concentration at the onset of solubilization has been found to be slightly lower than at the end. Recent theoretical calculations that take into account the finite size of micelles can explain this effect.)[49] When the mixed micelle region (region 3) is reached at $X_s = 0.66$ (X_s^{sol}) for C_{12}TAC and 0.64 for C_{14}TAC, there is again only one type of aggregate present, and the composition of the mixed micelles changes with total surfactant concentration. The slope of the curve in region 3 corresponds to a cmc of 8.4 mM assuming ideal mixing, slightly higher than the earlier determined value of 7.2 mM.[35] The corresponding values for C_{14}TAC and C_{16}TAC were 0.85 and 0.045 mM, respectively (Table 1).

A dip in the binding isotherm was obtained with C_{12}TAC, just before the first breakpoint. Although it was reproduced in several measurements, the dip is probably an artifact since there is no reason to believe that the amount of bound surfactant actually decreases prior to the onset of solubilization.

The binding isotherm of C_{16}TAC adsorption is shown in Figure 7c. Although no clear L_α/L_1 two-phase region is observed in the phase diagram of GMO/C_{16}TAB/ 100 mM NaCl[17] and no coexistence of vesicles and micelles was observed using cryo-TEM, the binding isotherm is strikingly similar to those of C_{12}-TAC and C_{14}TAC. Instead of a two-phase region, vesicles with pore defects were observed by cryo-TEM at surfactant concentrations just above the first breakpoint in the binding isotherm ($X_s = 0.57$). The nearly vertical slope implies that in the narrow region where these perforated vesicles exist, the chemical potential of the surfactant change little with increasing total

surfactant concentration, similarly to what was observed for the two-phase region with C_{12}TAC and C_{14}TAC.

The adsorption isotherm for the fluorinated surfactant, HFDePC, is shown in Figure 7d. At $X_s = 0.33$, the free surfactant concentration reaches the cmc, and micelles start to form, indicated by the steep rise of the amount of bound surfactant while the concentration of free surfactant remains the same. The lamellar−micellar coexistence region is very broad in this system: first after addition of surfactant to a molar ratio of approximately 50 all vesicles are solubilized as judged from the cryo-TEM investigation.

Discussion

Before discussing the results from the individual systems, we will present some theoretical considerations regarding the adsorption process. The distribution of surfactant between the aqueous pseudo-phase and the aggregates, which can be bilayers or mixed micelles, is determined by the chemical potential of the surfactant. In the aqueous phase, it is given by

$$\mu_{s,aq} = \mu_{s,aq}{}^0 + RT \ln[S]_f \quad (2)$$

In the aggregates, regarded as pseudo-phases, we have

$$\mu_{s,b} = \mu_{s,b}{}^0 + \gamma_b A_{s,b} + \mu_{s,b}{}^{el} + RT \ln X_s \quad (3)$$

where index b stands for bilayer.[47] The corresponding contributions for the mixed micelles are given by an equation of the same type, with index m (for micelles) instead of b. $\mu_{s,b}{}^0$ is the standard chemical potential of the surfactant in the bilayer, γ_b is the bilayer−water surface tension, $A_{s,b}$ is the area per surfactant in the bilayer, $\mu_{s,b}{}^{el}$ is the contribution to the chemical potential due to the electrostatic interactions of the surfactant headgroups in the bilayer, and X_s is the mole fraction of surfactant in the bilayer.

In the micelle case, there are further conditions and contributions. An entropy term that favors small micelles over large bilayers is given by

$$\frac{RT}{N}\ln[\text{mic}],$$

where N is the aggregation number. Important also is the constraint that the radius of the hydrophobic core of the (cylindrical or spherical) micelle cannot largely exceed the length of the fully stretched surfactant tail. The effect of this constraint is that the chemical potential of the surfactant in the micelles will increase sharply at a composition (below a certain fraction of the ionic component) where the optimal average amphiphile area is so low that the preferred radius of curvature becomes larger than the length of the surfactant tail. (It is also this constraint that explains the sphere to rod transition of the micelles.) Bearing in mind that these effects are neglected, as are also repulsive forces between the headgroups other than electrostatic, we proceed by using the equilibrium condition that the chemical potentials from eqs 2 and 3 are equal. Thus,

$$\ln\frac{X_s}{[S]_f} = \frac{1}{RT}(\mu_{s,aq}{}^o - \mu_{s,b}{}^o - \gamma_b A_{s,b} - \mu_{s,b}{}^{el}) = \ln K_b \quad (4)$$

where K_b is the partitioning coefficient for the surfactant between the bilayer and the aqueous solution. The coefficient, K_m, for partitioning between water and mixed micelles is defined correspondingly. The partitioning coefficients are not even in this approximation generally independent of the fraction, X_s, of surfactant in the aggregates. At a certain molar fraction of surfactant in the bilayer, commonly referred to as $X_s{}^{sat}$, the surfactant concentration in the aqueous phase reaches a level where mixed micelles start to form. $X_s{}^{sol}$ is used to denote the mole fraction of surfactant in the micelles when they first appear in the solution. With extra salt added so that the variations of the electrical free energy is small, and within a limited range of compositions close to the point where micelles at $X_s{}^{sol}$ and bilayers at $X_s{}^{sat}$ are at equilibrium, the change with composition in the value of the partitioning coefficient is small for both bilayers and mixed micelles. To show the principal behavior, we assume constant values of the coefficients and arrive in a behavior as sketched in Figure 8a,b. We discuss here the chemical potential of the surfactant, but also the chemical potential of the lipid must be the same in all phases at equilibrium. Since we do not attempt to calculate $X_s{}^{sol}$ and $X_s{}^{sat}$, this equality is ignored.

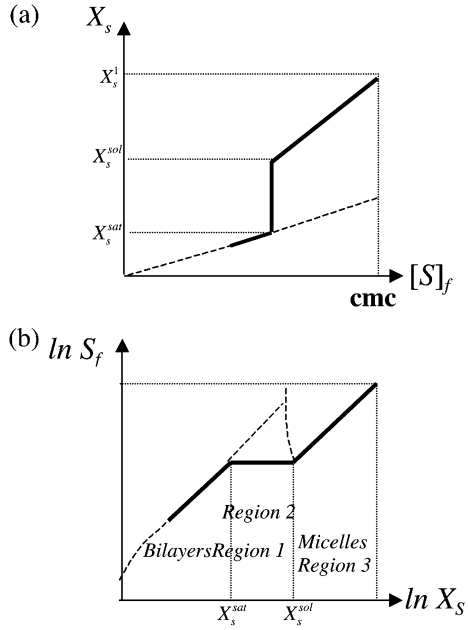

Figure 8. (a)Variation of X_s, the mole fraction of surfactant in aggregates, with $[S]_f$ according to eqs 4 and 5. The slope in the bilayer region is lower than in the micelle region. (b) $\ln[S]_f$, proportional to the chemical potential, is plotted vs $\ln X_s$.

The surfactant itself is known to form micelles in aqueous solutions. At $X_s = 1$, therefore, the micellar phase is the stable phase and forms when the free concentration of surfactant reaches the cmc. Bilayers at $X_s = 1$ would give a larger value of the surfactant chemical potential (due to a large repulsive energy from the headgroups) and therefore a larger free surfactant concentration.

In the micellar case, we have from eq 4

$$X_{s,m} = [S]_f K_m \quad (5)$$

with $K_m = 1/\text{cmc}$ ideally. For the bilayers, we obtain

$$X_{s,b} = [S]_f K_b \quad (6)$$

where $K_b < K_m$.

Figure 8a shows the variation of X_s with $[S]_f$ according to these equations and can be directly compared to the experimental results for C_{12}TAC and C_{14}TAC (Figure 7a,b). Eqs 5 and 6 were used to determine the distribution coefficients K_b and $K_m \approx 1/\text{cmc}$; the results are collected in Table 1.

The plot of Figure 8b uses the same relations and presents on the *y*-axis $\ln[S]_f$, linearly related to the chemical potential of the surfactant, and $\ln X_s$ as *x*-axis showing the change of the aggregate composition. Since the surfactants alone form micelles, we know that the chemical potential of the surfactant, and thus $[S]_f$, are lower for the micelles than for the bilayers at high X_s. According to eqs 4 and 5, therefore, the bilayers and micelles give two parallel straight lines with ideally a slope of unity in the representation of Figure 8b. Addition of the noncharged lipid to reduce X_s reduces the chemical potential of the surfactant (entropy of mixing). The uncharged lipid may be introduce without much change of the charge density but adds to the volume of the micelle core. This means that the radius of curvature of the micellar aggregates has to increase. In the case of the bilayers, the thickness must increase (from an unphysical thin state in the hypothetical bilayer with $X_s = 1$). At a certain value of X_s, the radius of curvature of the micellar aggregates would be larger than the length of the stretched lipid or surfactant tail; a further reduction of X_s would result in a rapid increase of the chemical potential of the surfactant in the micelles, as indicated in the plot. Under these conditions, formation of a bilayer becomes more favorable, and a transition from micelles to bilayers occurs.

The transition from cylindrical micelles to bilayer would be expected close to the point where the effective surfactant parameter, v/al, exceeds 0.5, which is the limit for cylinders with circular cross-section. In calculation of a value of the packing parameter, the length l is fixed, in this case, by the length of the stretched oleyl tail of the lipid, which is the longest tail in both cases. The mean area per amphiphile would be determined by the balance between the electrostatic headgroup repulsion of the charged surfactant and the hydrophobic forces.[48] At a fixed composition of the micelles, the surfactant headgroup area is expected to be almost the same with C_{12}TAC and C_{14}TAC. The only difference would then be the volume contributed by the surfactant tails, which is about 15% larger for the longer surfactant. The prediction would then be that more of the lipid is required to destabilize the micelles of the C_{12}—than of the C_{14}—surfactant, in accord with the values of X_s^{sol} found in the phase study (see Table 1).

In Figure 8a, the slope of the line in the bilayer region is smaller than in the micelle region. This is in accord with the experimental findings. The proportionalities described by eqs 4 and 5 are not found experimentally, however, probably due to the neglected effects mentioned previously. Further deviations from the predicted behavior are seen at high surfactant concentrations as the cmc/s of the surfactants in 100 mM NaCl are approached. The free surfactant concentration should equal the cmc at $X_s = 1$. However, as $X_s \rightarrow 1$, the surfactant concentration becomes very high, and its contribution to the ionic strength of the solution cannot be ignored, despite the presence of a relatively high concentration of a screening salt. A negative slope of the binding isotherm might therefore be observed in this region.

As presented, this model does not apply to the formation of holes in the bilayer in the case of C_{16}TAC. We can use it to explain the similar behavior of the adsorption isotherms also in this case by regarding the formation of holes as a cooperative process, in the same way as the formation of cylindrical micelles. Pores would start to form when a critical surfactant concentration is reached in the bilayer. The rims of the pores have a fixed surfactant-to-lipid ratio that is larger than that in the defect-free parts of the bilayer. Adding more surfactant would not alter this composition but result in an increased number of defects, similar to a vesicle−micelle phase separation. Finally, at relatively high surfactant concentrations, only edges remain in the form of entangled threadlike micelles. This process is schematically illustrated in Figure 9. There are, of course, further approximations involved, but still the main features of the observed isotherms can be understood.

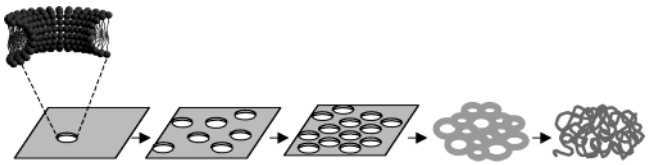

Figure 9. Schematic illustration of formation of pores in a bilayer. Pores start to form at a certain critical surfactant concentration, cpc, in the bilayer. Adding more surfactant leads to a higher density of pores until only pore edges remain in the form of threadlike micelles.

We expect the rim of the hole to be similar to (half of) a cylindrical micelle. Evidently, the radius of the pore must be larger than the half-thickness of the bilayer, so that the average curvature remains positive. We then expect the composition of the rim to be similar to that of the cylindrical micelles at the border of the micellar phase, whereas the bilayer between the pores would have a composition similar to the lamellar phase just before the pores start to form. These values should correspond to $X_s^{sat} \approx 0.57$ and $X_s^{sol} \approx 0.71$ in this case. The difference in composition between the rim of the pores and the bilayer is not large, therefore, which may explain why most efforts to monitor it have been unsuccessful. An exception was the highly decreased line splitting of a deuterium marked surfactant observed in the defective lamellar phase of the system EPC/C_{16}TAC/100 mM NaCl.[18,29]

Fluorinated, or partially fluorinated surfactants such as HFDePC mixed with normal hydrocarbon surfactants have been found to demix into two coexisting populations of micelles, one rich and the other poor in the fluorinated component.[30,50−53] It is obvious that fluorocarbon chains and hydrocarbon chains do not mix well. It is no surprise, therefore, that the mixed micelles of monoolein and HFDePC contain very little of GMO, explaining the large coexistence region. The bilayer, however, seems to accept a very significant amount of HFDePC, much more than the hydrocarbon rich micelles in mixtures of HFDePC with C_{16}TAC.[30,50,51] It appears as if the stiff FC tails mix better with the flexible HC chains in bilayers than in fluid solution[53] or micelles, maybe just because the chains in the bilayer are more aligned anyway. An interesting observation from the values of cmc and K_b in Table 1 is that the product of the two values for each surfactant is almost constant. This implies that the hydrophobicity of the fluorinated surfactant as measured on the scale set by the normal surfactants, is the same both when it is judged from the formation of the pure micelles and from the distribution of the surfactants into the GMO/surfactant bilayers, which again suggests that the nonideality of mixing between the hydrocarbon and the fluorocarbon surfactants is mainly found in the mixed micelles.

Conclusions

The most interesting features in the earlier investigated phase diagram of GMO/ C_{16}TAB/100 mM NaCl are the absence of a two phase area between the lamellar and micellar phases and the highly nonideal swelling of the perforated lamellar phase.[17] Both features were also found in the related mixture EPC/C_{16}TAC with salt.[18] The perforated vesicles observed by cryo-TEM in the present study of GMO/ C_{16}TAC/100 mM NaCl are regarded as a dispersion of this defective lamellar phase. In the

earlier studies, it was found that defect formation is promoted both by increasing surfactant concentration and by dilution. The constant activity of the surfactant throughout the perforated vesicle region supports the earlier suggested idea of segregation between the lipids and the surfactants within the perforated membrane resembling a phase transition.

It is not possible to point out a single simple reason for why perforated bilayers are formed with C_{16}TAC as surfactant but only mixed micelles with the two short chain analogues. In the model proposed for the formation of the pores, it is assumed that the rims of the pores are stabilized by surfactant-rich edges shaped as half-cylindrical micelles. It could be tempting to look for a reason here: in the solubilization of GMO with C_{12}TAC and C_{14}TAC, only globular micelles are observed, whereas C_{16}-TAC gives long cylindrical micelles. However, in the corresponding systems with EPC, cylindrical micelles do form in the solubilization with C_{12}TAC, but still neither perforated vesicles nor a defected lamellar phase are observed in this system.[29]

Another possibly important fact is that the mole fraction of surfactant accepted in the (defect-free) bilayer before defects or micelles are formed is the largest with the longest surfactant tail. Consequently, the charge density is also the highest in this case, which will have consequences for the electrostatic energy. Before this charge density has been reached with the two shorter-chain surfactants, the mixed micelles take over as the most favorable alternative. The free energy of the different options—perforated bilayers or coexisting micelles and vesicles—is probably rather close, so that a small difference can make the balance tip over. This assumption is corroborated by the observation of perforated vesicles as transient intermediates in the solubilization of EPC by sodium alkyl sulfates.[11]

Acknowledgment. Financial support from The Swedish Research Council is gratefully acknowledged. We thank Göran Karlsson for assistance in cryo-TEM experiments.

References and Notes

(1) Edwards, K.; Almgren, M. *J. Colloid Interface Sci*. **1991**, *147*, 1.
(2) Edwards, K.; Almgren, M.; Bellare, J.; Brown, W. *Langmuir* **1989**, *5*, 473.
(3) Vinson, P.; Talmon, Y.; Walter, A. *Biophys. J*., **1989**, *56*, 669.
(4) Paternostre, M. -T.; Roux, M.; Rigaud, J.-L. *Biochemistry* **1988**, *27*, 2668.
(5) Dennis, E. A. *Arch. Biochem. Biophys.* **1974**, *165*, 764.
(6) Kragh-Hansen, U.; le Maire, M.; Nöel, J. P.; Gulik-Krzywicki, T.; Møller, J. V. *Biochemistry* **1993**, *32*, 1648.
(7) Kragh-Hansen, U.; le Maire, M.; Møller, J. V. *Biophys. J*. **1998**, *75*, 2932.
(8) Rydhag, L.; Gabrán, T. *Chem. Phys. Lipids* **1982**, *30*, 309.
(9) Rydhag, L.; Stenius, P.; Ödberg, L. *J. Colloid Interface Sci.* **1982**, *86*, 274.
(10) Edwards, K.; Gustavsson, J.; Almgren, M.; Karlsson, G. *J. Colloid Interface Sci.* **1993**, *161*, 299.
(11) Silvander, M.; Karlsson, G.; Edwards, K. *J. Colloid Interface Sci.* **1996**, *179*, 104.
(12) Walter, A.; Vinson, P.; Kaplun, A.; Talmon, Y. *Biophys. J.* **1991**, *60*, 1315.
(13) Almog, S.; Kushnir, T.; Nir, S.; Lichtenberg, D. *Biochem.* **1986**, *25*, 2597.
(14) Schurtenberger, P.; Mazer, N.; Känzig, W. *J. Phys. Chem.* **1985**, *89*, 1042.
(15) Helenius, A.; Simons, K. *Biochim. Biophys. Acta* **1975**, *415*, 29.
(16) Lichtenberg, D.; Robson, R. J.; Dennis, E. A. *Biochim. Biophys. Acta* **1983**, *737*, 285.
(17) Gustafsson, J.; Orädd, G.; Nydén, M.; Hansson, P.; Almgren, M. *Langmuir* **1998**, *14*, 4987.
(18) Gustafsson, J.; Orädd, G.; Lindblom, G.; Olsson, U.; Almgren, M. *Langmuir* **1997**, *13*, 852.
(19) Hoffmann, H.; Thunig, C. H.; Munkert, U.; Meyer, H. W.; Richter, W. *Langmuir* **1992**, *8*, 2629.
(20) Quist, P. O.; Fontell, K.; Halle, B. *Liq. Crystals* **1994**, *16*, 235.
(21) Berger, K.; Hiltrop, K. *Colloid Polym. Sci.* **1996**, *274*, 269.
(22) Funari, S. S.; Holmes, M. C.; Tiddy, G. J. T. *J. Phys. Chem.* **1994**, *98*, 3015.
(23) Holmes, M. C.; Leaver, M. S.; Smith, A. M. *Langmuir* **1995**, *11*, 356.
(24) Leaver, M. S.; Holmes, M. C. *J. Phys. II* **1993**, *3*, 105.
(25) Ljusberg-Wahren, H.; Gustafsson, J.; Gunnarsson, T.; Krog, N.; Wannerberger, L.; Almgren, M. *Prog. Colloid Polym. Sci.* **1830**, *108*, 99.
(26) Kekicheff, P.; Cabane, B.; Rawiso, M. *J. Phys. Lett.* **1984**, *45*, 813.
(27) Berger, K.; Hiltrop, K. *Prog. Colloid Polym. Sci.* **1996**, *100*, 9.
(28) Heerklotz, H.; Seelig, J. *Biochim. Biophys. Acta* **2000**, *1508*, 69.
(29) Gustafsson, J.; Orädd, G.; Almgren, M. *Langmuir* **1997**, *13*, 6956.
(30) Asakawa, T.; Hisamatsu, H.; Miyagishi, S. *Langmuir* **1995**, *11*, 478.
(31) Dubochet, J.; Adrian, M.; Chang, J. J.; Homo, J. C.; Lepault, J.; McDowall, A. W.; Schultz, P. *Q. Rev. Biophys.* **1988**, *21*, 129.
(32) Bellare, J. R.; Davis, H. T.; Scriven, L. E.; Talmon, Y. J. *J. Electron Microsc. Technol.* **1988**, *10*, 87.
(33) Hayakawa, K.; Kwak, J. C. T. *J. Phys. Chem.* **1982**, *86*, 3866.
(34) Almgren, M.; Hansson, P.; Mukhtar, E.; van Stam, J. *Langmuir* **1992**, *8*, 2405.
(35) Kushner, L. M.; Hubbard, W. D.; Parker, R. A. *J. Res. Natl. Bur. Stand. (U.S.)* **1957**, *59*, 113.
(36) Johnson, S. B.; Drummond, C. J.; Scales, P. J.; Nishimura, S. *Colloids Surf. A* **1995**, *103*, 195.
(37) Schillén, K.; Brown, W.; Johnsen, R. M. *Macromolecules* **1994**, *27*, 4825.
(38) Gustafsson, J.; Nylander, T.; Almgren, M.; Ljusberg-Wahren, H. *J. Colloid Interface Sci.* **1999**, *211*, 326.
(39) Walter, A.; Vinson, P. K.; Talmon, Y. *Biophys. J.* **1991**, *60*, 1315.
(40) Egelhaaf, S. U.; Pedersen, J. S.; Schurtenberger, P. *Prog. Colloid Polym. Sci.* **1995**, *98*, 224.
(41) Small, D. M.; Bourges, M.; Dervichian, D. G. *Nature* **1966**, *211*, 816.
(42) Bagdassarian, C. K.; Roux, D.; Ben-Shaul, A.; Gelbart, W. M. *J. Chem. Phys.* **1991**, *94*, 3030.
(43) Porte, G.; Gomati, R.; Haitamy, O. E.; Apell, J.; Marignan, J. *J. Phys. Chem.* **1986**, *90*, 5746.
(44) Wang, K.; Karlsson, G.; Almgren, M.; Asakawa, T. *J. Phys. Chem.* **1999**, *103*, 9237.
(45) Balmbra, R. R.; Clunie, J. S.; Goodman, J. F. *Nature* **1969**, *222*, 1159.
(46) Mariani, P.; Luzzati, V.; Delacroix, H. *J. Mol. Biol.* **1988**, *204*, 165.
(47) Jönsson, B.; Wennerström, H. *J. Phys. Chem.* **1987**, *91*, 338.
(48) Israelachvili, J. *Intermolecular & Surface Forces*, 2nd ed.; Academic Press: San Diego, 1992.
(49) Lichtenberg, D.; Opatowski, E.; Kozlov, M. M. *Biochim. Biophys. Acta* **2000**, *1508*, 1.
(50) Kadi, M.; Hansson, P.; Almgren, M.; Furo, I. *Langmuir* **2002**, *18*, 9243.
(51) Almgren, M.; Wang, K.; Asakawa, T. *Langmuir* **1997**, *13*, 4535.
(52) Carlfors, J.; Stilbs, P. *J. Phys. Chem.* **1984**, *88*, 4410.
(53) Asakawa, T.; Imae, T.; Ikeda, S.; Miyagishi, S.; Nishida, M. *Langmuir* **1991**, *7*, 262.
(54) Shinoda, K.; Nomura, T. *J. Phys. Chem.* **1980**, *84*, 365.